

Implementable Quantum Classifier for Nonlinear Data

Yuxuan Du,^{1,*} Min-Hsiu Hsieh,^{2,†} Tongliang Liu,^{1,‡} Dacheng Tao^{1,§}

¹*UBTECH Sydney Artificial Intelligence Centre and the School of Information Technologies,
Faculty of Engineering and Information Technologies, The University of Sydney, Australia*

²*Centre for Quantum Software and Information,
Faculty of Engineering and Information Technology, University of Technology Sydney, Australia*
(Dated: September 18, 2018)

In this Letter, we propose a quantum machine learning scheme for the classification of classical nonlinear data. The main ingredients of our method are variational quantum perceptron (VQP) and a quantum generalization of classical ensemble learning. Our VQP employs parameterized quantum circuits to learn a Grover search (or amplitude amplification) operation with classical optimization, and can achieve quadratic speedup in query complexity compared to its classical counterparts. We show how the trained VQP can be used to predict future data with $O(1)$ query complexity. Ultimately, a stronger nonlinear classifier can be established, the so-called quantum ensemble learning (QEL), by combining a set of weak VQPs produced using a subsampling method. The subsampling method has two significant advantages. First, all T weak VQPs employed in QEL can be trained in parallel, therefore, the query complexity of QEL is equal to that of each weak VQP multiplied by T . Second, it dramatically reduce the runtime complexity of encoding circuits that map classical data to a quantum state because this dataset can be significantly smaller than the original dataset given to QEL. This arguably provides a most satisfactory solution to one of the most criticized issues in quantum machine learning proposals. To conclude, we perform two numerical experiments for our VQP and QEL, implemented by Python and pyQuil library. Our experiments show that excellent performance can be achieved using a very small quantum circuit size that is implementable under current quantum hardware development. Specifically, given a nonlinear synthetic dataset with 4 features for each example, the trained QEL can classify the test examples that are sampled away from the decision boundaries using 146 single and two qubits quantum gates with 92% accuracy.

In machine learning, Perceptron can be efficiently constructed to learn a decision rule that classifies linear data with binary classes [1]. Mathematically, a labeled training dataset \mathcal{D} with N examples is denoted as $\mathcal{D} = \{(\mathbf{x}_i, y_i)\}_{i=1}^N$, where $\mathbf{x}_i \in \mathbb{R}^M$ represents the i -th data vector with M features and $y_i \in \{-1, 1\}$ represents the corresponding label. A perceptron aims to learn a hyperplane $W \in \mathbb{R}^M$ that can accurately classify dataset \mathcal{D} in the sense that W minimizes $\sum_{i=1}^N -\text{sign}(y_i W \mathbf{x}_i)$.

Perceptron can be used as a building block for various advanced machine learning methods, such as the classification of nonlinear data. This capability of classifying nonlinear data enables Perceptron to be broadly applied to a majority of practical learning tasks, e.g., image classification and data mining [2–5].

The learning model that employs multiple Perceptrons to learn nonlinear data can be built by two strategies. First, by laying out Perceptrons to mimic the neural network structure and introducing an activation function [6], the proposed Multilayer Perceptron [7] is capable of approximating any function [8]. Second, in contrast to using one learning model to learn all the features from the training data, the proposed ensemble methods [9] employ T weak learners (Perceptrons) to learn different features from nonlinear data and combine them into a strong classifier with a combining rule, e.g., the majority voting rule [9].

As one of the most demanded applications of quantum

computers, quantum machine learning aims to solve specific learning tasks that cannot be efficiently solved by classical computers [10]. Considering the significance of Perceptron in classical machine learning, a quantum Perceptron algorithm with quantum advantages is desirable.

Previous results in quantum Perceptron requires an expensive number of qubits and unaffordable circuit size. The Quantum Perceptron proposed in [11] demands a deep circuit to conduct phase estimation, and the Quantum Perceptron proposed in [12] demands an immense number of quantum gates proportional to the size of training data. Quantum Perceptron proposed in [13] also requires an enormous number of qubits to encode classical data, and employs the Grover oracle, although it is not explicitly explained. In other words, using near-term quantum devices with a limited number of qubits and a shallow circuit depth to implement the above quantum Perceptron proposals is impractical.

In this paper, we propose variational quantum Perceptron (VQP) to resolve the aforementioned issues. Our VQP employs a classical optimizer to iteratively update the trainable parameters of a quantum learning circuit. A decision rule can be obtained with $O(\text{poly}(\log M)\sqrt{N})$ query complexity, where N is the sample size and M is the number of features of each example. An asymptotically quadratical speedup can be achieved over its classical counterparts if $\text{poly}(\log M) \ll N$. Moreover, the number of required input qubits is $O(\log(MN))$, logarithmically

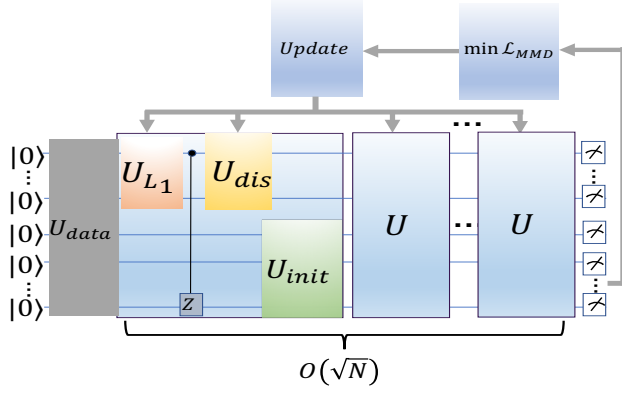


FIG. 1: The quantum circuit of VQP. After the first cycle, U_{L1} is substituted by U_{dis}^\dagger , i.e., $U := U_{dis}^\dagger \circ CZ \circ U_{dis} \circ U_{init}$.

proportional to the number of features and the sample size. We also show that our trained VQP can predict the future label of new input data with $O(1)$ query complexity.

Our second contribution is that we propose the quantum ensemble learning (QEL) method to solve more complex tasks, such as the nonlinear dataset. In contrast to previous studies that employ quantum Perceptron as the basic element for building neural networks to accurately classify nonlinear data [12, 14, 15], QEL is more flexible for accomplishing such tasks and can be easily implemented on near-term quantum devices. Our numerical experiments confirm that QEL can be used to classify a nonlinear dataset on small scale quantum circuits. Multiple weaker VQPs are combined to learn different features of training dataset. By employing a subsampling method to train T weak learners in parallel whose size of the training subset is $poly(\log N)$, the query complexity and runtime complexity of QEL are $O(T poly(\log M \sqrt{\log N}))$ and $O(poly(\log M \log(M \log N))\sqrt{\log N})$, respectively.

Variational Quantum Perceptron.—A crucial component of our scheme is the variational quantum Perceptron (VQP), which consists of three quantum blocks and a classical optimizer. VQP employs parametrized quantum circuits (PQC) to learn features from the training data and exploits the learned decision rule to guide a Grover-like search algorithm to identify the index of the mislabeled example. Recall that Grover search [16] (or amplitude amplification (AA) [17]) identifies the k -th element by iteratively applying a predefined oracle $U_f = \mathbb{I} - 2|k\rangle\langle k|$ and a diffusion operator $U_{init} = \mathbb{I} - 2/N \sum_i |i\rangle\langle i|$ to the input state. In VQP, a trainable PQC is used to replace the oracle U_f , followed by U_{dis} , which is specifically designed for our data structure. Both units are data-driven using a classical optimization approach. Lastly, U_{init} is applied and one cycle is completed. The mislabeled example can be sampled with a high probability after $O(\sqrt{N})$ cycles, where N is the size of the input data. The implementation of VQP is illustrated in Figure 1.

Given a classical dataset $\mathcal{D} = \{(\mathbf{x}_i, y_i)\}_{i=1}^N \in (\mathbb{R}^{N \times M}, \{-1, 1\}^N)$ with N examples and M features in each example, VQP first constructs a mislabeled dataset $\mathcal{D}_k = \{(-y_k \mathbf{x}_k)\} \cup \{(y_i \mathbf{x}_i)\}_{i \neq k}^N$ by mislabeling the sign of the k -th outcome y_k before multiplying it by \mathbf{x}_k . Then, \mathcal{D}_k is encoded into a quantum state $|\Phi^k\rangle_{F,I} = 1/\sqrt{N} \sum_{j=0}^{M-1} (\sum_{i \neq k} y_i x_{ji} |j\rangle_F |i\rangle_I - y_k x_{jk} |j\rangle_F |k\rangle_I)$, where w.l.o.g. $\sum_j |y_i x_{ji}|^2 = 1/N$, $\forall i \in \{0, 1, \dots, N-1\}$. We remark that this step is unavoidable in most quantum machine learning proposals. The quantum state $|\Phi^k\rangle_{F,I}$ consists of two quantum subsystems: a feature register \mathcal{R}_F with $\lceil \log M \rceil$ qubits and an index register \mathcal{R}_I with $\lceil \log N \rceil$ qubits. For simplicity, we only report treating the training dataset with uniform distribution in the main text, and cover the non-uniform distribution datasets in the supplemental material SM(A).

As discussed in [18], combining a variational learning approach with Grover search produces additional quantum advantages, i.e., variational search has a higher probability of success than conventional Grover's algorithm in finding the solution. A similar idea is used in VQP, where parametrized quantum circuits (PQCs) are employed to learn the mislabeled index k from the data feature. With slight abuse of notation, the PQC U_f is composed of two parts: a $U_{L1} = \prod_{i=1}^{L1} U(\theta^i)$ applied to the feature register \mathcal{R}_F followed by a CZ gate (the blue region in Figure 1), where each block $U(\theta^i)$ contains $O(\lceil \log M \rceil)$ trainable parameterized single qubit gates and at most $\lceil \log M \rceil$ CNOT gates with the same layouts. In the optimal learning situation, U_{L1} yields the following target state:

$$(U_{L1} \otimes \mathbb{I}_I) |\Phi^k\rangle_{F,I} = \frac{1}{\sqrt{N}} \left(\sum_{i=0, i \neq k}^{N-1} |\psi_i^{(0)}\rangle_F |i\rangle_I + |\psi_k^{(1)}\rangle_F |k\rangle_I \right), \quad (1)$$

where $|\psi_i^{(0)}\rangle_F$ (resp. $|\psi_k^{(1)}\rangle_F$) denotes the first qubit of the quantum state in the feature register \mathcal{R}_F that is indexed by i (resp. k), being $|0\rangle$ (resp. $|1\rangle$). Applying the CZ gate to the index register controlled by the first qubit of the feature register yields

$$U_f |\Phi^k\rangle_{F,I} = \frac{1}{\sqrt{N}} \left(\sum_{i=0, i \neq k}^{N-1} |\psi_i^{(0)}\rangle_F |i\rangle_I - |\psi_k^{(1)}\rangle_F |k\rangle_I \right). \quad (2)$$

Analogous to the U_f in Grover search, the trainable and data-driven U_f in Eqn. (2) also conditionally flips the phase of the mislabeled target.

In contrast to Grover search, VQP has an additional feature register that encodes information about the data features. Naively applying the diffusion operation $U_{init} = \mathbb{I} - 2/N \sum_i |i\rangle\langle i|_I$ will not work because entanglement exists between the index and feature registers. To fix this problem, a disentangled operator U_{dis} is needed before

U_{init} is applied. Such an operator $U_{dis} = \prod_{i=1}^{L_2} U(\theta^i)$ is constructed by another PQC that contains L_2 blocks. In the optimal solution, U_{dis} yields the following disentangled state:

$$(U_{dis} \otimes \mathbb{I})U_f |\Phi^k\rangle_{F,I} = |\Phi^k\rangle_F \otimes \frac{1}{\sqrt{N}} \left(\sum_{i \neq k} |i\rangle_I - |k\rangle_I \right) \quad (3)$$

where $|\Phi^k\rangle_F = \sum_{j=0}^{M-1} x'_j |j\rangle_F$ is some quantum state of the feature register with $\sum_j |x'_j|^2 = 1$.

Since the quantum state in Eqn. (3) is separable, the diffusion operator U_{init} can be applied to \mathcal{R}_I , and the probability amplitude of $|k\rangle_I$ will be increased as it is in Grover search. Mathematically, the state defined in Eqn. (3) can be reformulated as $|\Phi^k\rangle_F \otimes (\sqrt{(N-1)/N} |B\rangle_I - 1/\sqrt{N} |A\rangle_I)$, with $|B\rangle_I := 1/\sqrt{N-1} \sum_{i \neq k} |i\rangle_I$ and $|A\rangle_I := |k\rangle_I$. The generated state after applying U_{init} is

$$\begin{aligned} & (\mathbb{I} \otimes U_{init})(U_{dis} \otimes \mathbb{I})U_f |\Phi^k\rangle_{F,I} \\ &= |\Phi^k\rangle_F \otimes (\cos 3\theta |B\rangle_I + \sin 3\theta |A\rangle_I) \end{aligned} \quad (4)$$

where $\sin \theta := \sqrt{1/N}$. This completes the first iteration of VQP.

Denote U as the composition of U_{dis}^\dagger , CZ , U_{dis} , and U_{init} [19]. The probability amplitude of the objective $|A\rangle$ will be $\sin((2\ell + 1)\theta)$ after subsequently applying U ℓ times. Therefore, when $\ell \approx (\pi - 2\theta)/4\theta$, or $\ell \sim O(\sqrt{N})$, the probability of $|A\rangle$ is maximized to 1, and the VQP is learned successfully. Note that we leave discussion of the classical optimization process to the supplementary materials SM(B).

Robustness of VQP.—There are two crucial factors that influence the performance of VQP, namely, the imperfection of the trained U_{L_1} and that of U_{dis} . Notably, the aforementioned two factors can be reduced to one problem as follows. How many blocks of a parametrized quantum circuit are required to generate a desired quantum state? It is shown in [20], that employing $O(\text{poly}(\log M))$ blocks in PQCs is capable of approximating any quantum state up to ϵ -error in trace distance. The following theorem guarantees that a small error ϵ of the generated state in VQP does not significantly influence performance. The proof is given in supplementary materials SM(C).

Theorem 1. *Suppose that, for an optimal VQP, the success probability of identifying the mislabeled index k , after $S \sim O(\sqrt{N})$ iterations, is p . After training, the success probability using such a noisy VQP satisfies $q = |(1 - \epsilon)|^S p$.*

VQP Application in Prediction.—Once the training of U_{L_1} has finished, VQP can be directly employed to predict future instances with query complexity equal to $O(1)$. To achieve this, we propose the following prediction method, inspired by the SWAP test [21]. We denoted the

new input as $\tilde{\mathbf{x}}$. The new input and the mislabeled data $-y_k \mathbf{x}_k$ are first encoded into an entangled quantum state as follows:

$$|\psi\rangle_{F,I} = \frac{1}{\sqrt{2}} \left(\sum_{j=0}^{M-1} \tilde{x}_j |j\rangle_F |0\rangle_I + \sum_{j=0}^{M-1} -y_k x_{jk} |j\rangle_F |1\rangle_I \right). \quad (5)$$

Applying the trained $U_{L_1} \otimes \mathbb{I}_I$ and $\mathbb{I} \otimes H$ to $|\psi\rangle_{F,I}$ gives

$$\begin{aligned} & U_{L_1} \otimes H |\psi\rangle_{F,I} = \\ & \frac{1}{2} \left(|\tilde{\psi}\rangle_F + |\psi_k^{(1)}\rangle_F \right) |0\rangle_I + \frac{1}{2} \left(|\tilde{\psi}\rangle_F - |\psi_k^{(1)}\rangle_F \right) |1\rangle_I, \end{aligned} \quad (6)$$

where $|\tilde{\psi}\rangle_F = U_{L_1} \sum_{j=0}^{M-1} \tilde{x}_j |j\rangle_F$. We rewrite $|\tilde{\psi}\rangle_F$ as follows:

$$|\tilde{\psi}\rangle_F = \alpha |\tilde{\psi}^{(0)}\rangle_F + \beta |\tilde{\psi}^{(1)}\rangle_F, \quad (7)$$

where $|\alpha|^2 + |\beta|^2 = 1$. If $\tilde{\mathbf{x}}$ is close to $y_k \mathbf{x}_k$, namely $\|\tilde{\mathbf{x}} - y_k \mathbf{x}_k\|^2 < \epsilon$, we have $\beta \rightarrow 1$ and $|\tilde{\psi}^{(1)}\rangle_F \rightarrow |\psi_k^{(1)}\rangle_F$. We fix a success probability threshold C_T . The new input data $\tilde{\mathbf{x}}$ will then be identified as mislabeled, i.e., the classified label is -1 , if the probability of obtaining the outcome 10 is larger than C_T after measuring the first qubit of the feature register and the index register.

We remark that, without the additional H gate in Eqn. (6), U_{L_1} alone followed by measuring the aforementioned qubits will not be able to classify the new input data since U_{L_1} only introduces a global phase when acting upon the mislabeled state. The introduced SWAP test in Eqn. (6) allows us to circumvent this issue.

Classification of Nonlinear Data.—Hampered by the linearity of quantum mechanics, a critical question in quantum machine learning is how to efficiently learn a nonlinear and large size dataset (industrial dataset). The literature mainly focuses on building quantum neural networks and developing techniques to encompass crucial nonlinearity into quantum circuits [12, 14, 22–25]. However, these proposals are still far from implementable in near-term quantum devices. In this Letter, we address this problem using the quantum generalization of a classical ensemble learning method. A homogeneous quantum ensemble learning (QEL) is employed [9], in which all weak learners of QEL are constructed by VQP.

Given a training dataset \mathcal{D} of size N , T smaller datasets $\{\mathcal{D}_t\}_{t=1}^T$ are first created via the subsampling method [26], i.e., each \mathcal{D}_t is constructed by randomly sampling rN examples from \mathcal{D} with the ratio $r \in (0, 1)$ [27]. $\{\mathcal{D}_t\}_{t=1}^T$ are then employed to train T weak VQPs $\{V_t\}_{t=1}^T$ with success probabilities $\{p_t\}_{t=1}^T$, respectively. Note that this step can be accomplished in parallel. The sampling ratio r then determines the trade-off between the accuracy of the data classification and the overall efficiency.

Nonlinear data are classified as follows. Fix the threshold C_T for T weak learners. For each new input $\tilde{\mathbf{x}}$, the

trained weak VQPs $\{V_t\}_{t=1}^T$ are used to predict its labels, where the predicted labels and the corresponding success probabilities are denoted as $\{y_t\}_{t=1}^T$ and $\{p_t\}_{t=1}^T$, respectively. A scale parameter S_c is introduced to increase the belief of the predicted label. For each weak learner, when $y_k = y_t$, the belief is $S_c \times y_t |p_t - C_T|$, with $S_c > 1$, otherwise the belief is 0 with $S_c = 0$ [28]. Given an input \mathbf{x} , the strong classifier H is defined as $H(\mathbf{x}) = \text{sign}(\sum_{t=1}^T S_c \times y_t |p_t - C_T|)$, with $H(\mathbf{x}) \in \{-1, 1\}$.

The query complexity of our proposed QEL is equal to the query complexity of training each of the weak VQP V_t by multiplying a small constant T : $O(T \text{poly}(\log M) \sqrt{|\mathcal{D}_t|})$, where M is the feature size and $|\mathcal{D}_t|$ is the size of the training dataset for V_t . The runtime complexity of QEL is $O(\text{poly}(\log M \log(M|\mathcal{D}_t))) \sqrt{|\mathcal{D}_t|}$, where $\text{poly}(\log(M|\mathcal{D}_t))$ represents the runtime of encoding classical data into quantum circuits. This is because all T VQP $\{V_t\}_{t=1}^T$ can be trained in parallel and the oracle only includes $\text{poly}(\log M)$ gates. When the dataset \mathcal{D}_t is large, our approach will have a huge advantage over classical subsampling ensemble learning, whose query complexity is $O(|\mathcal{D}_t|)$. Additionally, our method allows the size of the dataset \mathcal{D}_t to be traded for the efficiency of preparing a quantum state from classical data. This could potentially resolve the most critical issue confronting quantum machine learning.

Numerical Experiments.— The first experiment demonstrates the performance of our VQP in learning a linearly separable training dataset \mathcal{D} . Consider a synthetic dataset \mathcal{D} that includes 8 examples and 4 features for each example. The 8 examples of \mathcal{D} are $\mathcal{D} = \{(\mathbf{x}_i, y_i)\}_{i=1}^8$ with $(\mathbf{x}_1 = [0.6, 0.8, -1/\sqrt{2}, -1/\sqrt{2}], y_1 = 1)$, $(\mathbf{x}_2 = [1, 0, -1/\sqrt{3}, -\sqrt{2}/3], y_2 = 1)$, $(\mathbf{x}_3 = [0, 1, -1/3, -\sqrt{8}/3], y_3 = 1)$, $(\mathbf{x}_4 = [1/2, \sqrt{3}/2, -1, 0], y_4 = 1)$, $(\mathbf{x}_5 = [0.8, 0.6, -\sqrt{3}/3, -\sqrt{6}/3], y_5 = 1)$, $(\mathbf{x}_6 = [\sqrt{6}/7, 1/\sqrt{7}, -\sqrt{5}/5, -\sqrt{20}/5], y_6 = 1)$, $(\mathbf{x}_7 = [-\sqrt{3}/3, -\sqrt{3}/6, 0.6, 0.8], y_7 = -1)$, and $(\mathbf{x}_8 = [-\sqrt{3}/3, -\sqrt{3}/6, 0.6, 0.8], y_8 = 1)$. Note that \mathcal{D} is linearly separable since a hyperplane $W = [a_1, a_2, a_3, a_4]$ with $a_1, a_2 < 0$ and $a_3, a_4 > 0$ can accurately classify all examples in \mathcal{D} , i.e., $y_i W \mathbf{x}_i \geq 0, \forall i \in [1, 8]$. The dataset \mathcal{D} can be encoded into a quantum state with three index qubits and two feature qubits. We create a dataset \mathcal{D}_8 in which we deliberately mislabel the 8th example (i.e., $y_8 = 1$). Following the encoding method of VQP, the dataset \mathcal{D}_8 is encoded into the quantum state $|\Phi^8\rangle$.

The numerical simulations are implemented in Python in conjunction with the pyQuil library [29]. The detailed setting used in our experiment is as follows. The oracle U is queried $O(\sqrt{|\mathcal{D}|}) \approx 3$ times. The number of quantum circuit blocks in training U_f, U_{dis} is set to $L_1 = L_2 = 3$ and $L_1 = L_2 = 5$, respectively. The number of iterations used in the classical optimization in training U_f, U_{dis} is set at 100 and the number of measurements in each iteration is set at 20. The bandwidth parameter of MMD loss

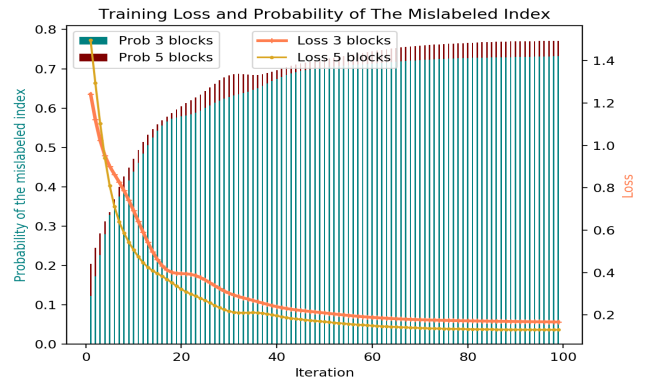


FIG. 2: The training loss and probability of the mislabeled index with different settings.

and the learning rate are set as 0.3 and 0.02, respectively (see supplemental material SM(B) for details). We plot, in Figure 2, the MMD loss and the successful probability of sampling the mislabeled index versus the number of classical iterations, and show that increasing the number of blocks contributes to fast convergence and higher successful probability. MMD loss and the successful probability after the full iteration is 0.1767 and 0.1158, 72.59% and 78.46%, for the case $L_1 = L_2 = 3$ and $L_1 = L_2 = 5$, respectively.

A test dataset including 100 examples is employed to evaluate the performance of the trained U_{L_1} . All test examples are sampled from the distribution \mathcal{V} to guarantee $y_i W \mathbf{x}_i > 0$, where $\mathcal{V} \sim [\cos \alpha, \sin \alpha, \cos \beta, \sin \beta]$ and $(\alpha, \beta) \in ([0, \pi/2], [\pi, 3\pi/2])$ for $y_i = 1$ and $(\alpha, \beta) \in ([\pi, 3\pi/2], [0, \pi/2])$ for $y_i = -1$. According to the prediction method, we set the threshold C_T as 0.50, 0.60, and 0.65. The test accuracy for the $L_1 = L_2 = 3$ case is 100%, 100%, and 97%, respectively, and for the $L_1 = L_2 = 5$ case, it is 100%, 100%, and 96.5%, respectively.

We investigate how our VQP performs under quantum circuit gate noise. As shown in Figure 3, when the gate noise probability is $n_2 = 0.025\%$, the MMD loss still converge and the successful probability of sampling the mislabeled index degrades only slightly compared with the noise free case. However, the performance of our VQP becomes poor when the circuit noise is $n_1 = 0.1\%$.

Our second experiment demonstrates how well our QEL classifies a synthetic nonlinear dataset. Consider the training dataset $\mathcal{D} = \{\mathbf{x}_i, y_i\}_{i=1}^{10000}$ with $|\mathbf{x}_i| = 4$ and $y_i \in \{-1, 1\}$. This nonlinear dataset \mathcal{D} is constructed as follows: with $(\theta_{1i}, \theta_{2i}) \in ([0, \pi], [0, \pi])$, the data $\mathbf{x}_i = [\cos \theta_{1i}, \sin \theta_{1i}, \cos \theta_{2i}, \sin \theta_{2i}]$ and the label is $y_i = -1$ if and only if $\theta_{1i} \in [\pi/3, 2\pi/3]$, otherwise $y_i = 1$.

The number of weak learners $\{V_t\}_{t=1}^T$ is set to $T = 4$, and the size of the data subset \mathcal{D}_t is set to $|\mathcal{D}_t| = 8$, i.e., the subsampling ratio is $r = 0.0008$. The first two features of the training data and 4 sub-datasets are shown in Figure 4 (a). Two decision boundaries are required to classify

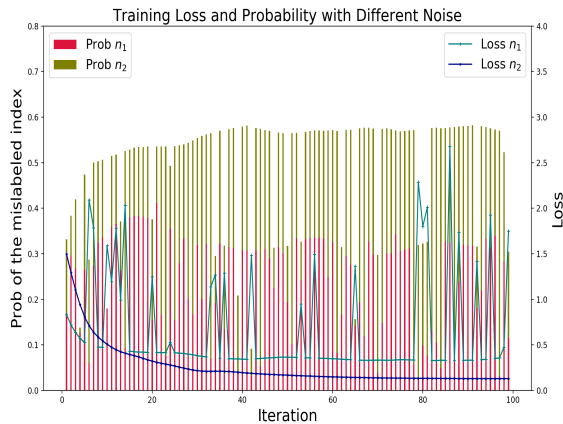


FIG. 3: The training loss and the successful probability of sampling the mislabeled index under two noise settings $n_1 = 0.1\%$ and $n_2 = 0.025\%$, with the setting $L_1 = L_2 = 3$.

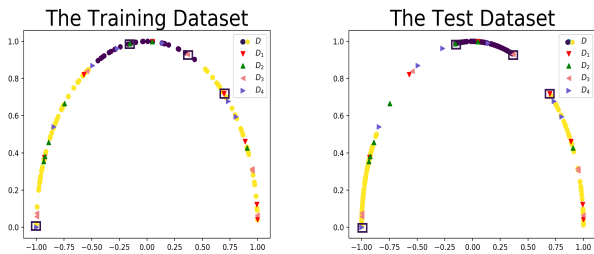


FIG. 4: The left figure illustrates the first two features of the training dataset and 4 sub-datasets. The yellow and purple points represent the label $y = 1$ and $y = -1$, respectively. The mislabeled example for each subset is indicated by the black box. The right figure illustrates another test dataset to further validate the performance of QEL, where the first two features of all test data are far away from the class margins.

such a nonlinear dataset. The number of index qubits and feature qubits of each V_i is 3 and 2, respectively. The number of blocks is set as $L_1 = L_2 = 3$. The bandwidth parameter of MMD loss and the learning rate are set as 0.3 and 0.02, respectively.

After training, a new test dataset with 300 examples is constructed. We employ the belief majority voting rule to build a strong classifier H , in which the scale parameter S_c is set to 5. As explained in supplementary materials SM(D) that a higher threshold for $y_k = -1$ and a lower threshold for $y_k = 1$ will make VQP focus on the local features, thus the C_T is set as 0.1 and 0.5 for $y_k = 1$ and $y_k = -1$, respectively. As illustrated in Table II, the classification accuracy of the combined strong classifier will increase and outperform the single weak learner. Since the training data of all sub-datasets are far away from the class margins, the strong classifier cannot accurately classify the test points located in this region. To further validate the performance of QEL, as illustrated in Figure 4

TABLE I: Nonlinear Model Results

	V_1	V_2	V_3	V_4	$\{V_i\}_{i=1}^4$
Acc $y_t = 1$ (%)	56.00	0.03	0.02	68.66	80.33
Acc $y_t = -1$ (%)	47.00	100.00	100.00	39.00	82.33
Acc $y_t = \pm 1$ (%)	51.50	50.02	50.01	53.83	81.33

TABLE II: The Acc represents the accuracy of classifying the test data. $y_t = -1$, $y_t = 1$, and $y_t = \pm 1$ represent all labels of test examples are -1 , $+1$ and uniformly mixed, respectively.

(b), another test dataset that all test examples are sampled away from decision boundaries is employed. Using the same 4 weak learners, the classification accuracy of QEL for this dataset is improved to 92%. In the training process, 29 single and two qubits gates are averagely required to encode 8 examples into quantum circuits. Then, 36 parameterized single qubit gates, 6 CNOT gates, 3 CZ gates, 24 Hadamard gates, and 3 Toffoli gates (can be decomposed into 10 singles qubit gates and 6 CNOT gates) are employed to build all oracles. Alternatively, the QEL is implemented by total 146 single and two qubits gates.

Discussion and Conclusion.—In this Letter, we have proposed VQP, which achieves quadratic speedup in query complexity over its classical counterparts. We have also proposed QEL for the classification of nonlinear data, using a set of weaker VQP as building blocks. Our QEL scheme has great overall query complexity and runtime complexity at the state preparation stage. Our numerical experiments show that excellent performance can be achieved even with a small quantum circuit size. We believe this will provide immediate and practical applications for near term quantum devices.

This research is supported by ARC projects FL-170100117 and DP-180103424. MH is supported by an ARC Future Fellowship under Grant FT140100574. The Python codes for our experiments are available upon request.

* yudu5543@uni.sydney.edu.au

† Min-Hsiu.Hsieh@uts.edu.au

‡ tongliang.liu@sydney.edu.au

§ dacheng.tao@sydney.edu.au

- [1] F. Rosenblatt, *Psychological Review* **65**, 386 (1958).
- [2] R. O. Duda, P. E. Hart, and D. G. Stork, *Pattern Classification* (John Wiley & Sons, 2012).
- [3] T. Hastie, R. Tibshirani, and J. Friedman, in *The elements of statistical learning* (Springer, 2009) pp. 485–585.
- [4] R. M. Haralick, K. Shanmugam, *et al.*, *IEEE Transactions on systems, Man, and Cybernetics*, 610 (1973).

- [5] I. H. Witten, E. Frank, M. A. Hall, and C. J. Pal, *Data mining: Practical machine learning tools and techniques* (Morgan Kaufmann, 2016).
- [6] M. Leshno, V. Y. Lin, A. Pinkus, and S. Schocken, *Neural Networks* **6**, 861 (1993).
- [7] K. Hornik, M. Stinchcombe, and H. White, *Neural Networks* **2**, 359 (1989).
- [8] J. Schmidhuber, *Neural Networks* **61**, 85 (2015).
- [9] T. G. Dietterich, in *International Workshop on Multiple Classifier Systems* (Springer, 2000) pp. 1–15.
- [10] J. Biamonte, P. Wittek, N. Pancotti, P. Rebentrost, N. Wiebe, and S. Lloyd, *Nature* **549**, 195 (2017).
- [11] M. Schuld, I. Sinayskiy, and F. Petruccione, *Physics Letters A* **379**, 660 (2015).
- [12] E. Torrontegui and J. J. Garcia-Ripoll, arXiv preprint arXiv:1801.00934 (2018).
- [13] A. Kapoor, N. Wiebe, and K. Svore, in *Advances in Neural Information Processing Systems* (2016) pp. 3999–4007.
- [14] M. Schuld, I. Sinayskiy, and F. Petruccione, *Quantum Information Processing* **13**, 2567 (2014).
- [15] A. Narayanan and T. Menneer, *Information Sciences* **128**, 231 (2000).
- [16] L. K. Grover, in *Proceedings of the Twenty-eighth Annual ACM Symposium on Theory of Computing* (ACM, 1996) pp. 212–219.
- [17] G. Brassard, P. Hoyer, M. Mosca, and A. Tapp, arXiv preprint quant-ph/0005055 (2000).
- [18] M. E. Morales, T. Tlyachev, and J. Biamonte, arXiv preprint arXiv:1805.09337 (2018).
- [19] The reason of applying U_{dis}^\dagger is to revert the state back into the entangled state as defined in Eqn. (2) so that applying CZ gate can conditionally flip the $|k\rangle_I$ again.
- [20] Y. Du, M.-H. Hsieh, T. Liu, and D. Tao, In preparation.
- [21] H. Buhrman, R. Cleve, J. Watrous, and R. De Wolf, *Physical Review Letters* **87**, 167902 (2001).
- [22] E. Farhi and H. Neven, arXiv preprint arXiv:1802.06002 (2018).
- [23] M. Schuld, A. Bocharov, K. Svore, and N. Wiebe, arXiv preprint arXiv:1804.00633 (2018).
- [24] K. H. Wan, O. Dahlsten, H. Kristjánsson, R. Gardner, and M. Kim, *npj Quantum Information* **3**, 36 (2017).
- [25] N. Killoran, T. R. Bromley, J. M. Arrazola, M. Schuld, N. Quesada, and S. Lloyd, arXiv preprint arXiv:1806.06871 (2018).
- [26] P. Bühlmann, B. Yu, *et al.*, *The Annals of Statistics* **30**, 927 (2002).
- [27] In the sampling process, it is best that the T mislabeled examples should be spread across all classes to learn different features.
- [28] $S_c \times y_t |p_t - C_T|$ can be viewed as the confidence of the prediction produced by the t -th weak VQP V_t , where a higher p_t implies that the new input is more likely to be mislabeled. On the other hand, a lower p_t implies that the new input is more likely to be correctly labeled. Generally, S_c is proportional to the number of weak learners.
- [29] R. S. Smith, M. J. Curtis, and W. J. Zeng, arXiv preprint arXiv:1608.03355 (2016).
- [30] M. Benedetti, D. Garcia-Pintos, Y. Nam, and A. Perdomo-Ortiz, arXiv preprint arXiv:1801.07686 (2018).
- [31] J.-G. Liu and L. Wang, arXiv preprint arXiv:1804.04168 (2018).
- [32] M. Benedetti, J. Realpe-Gómez, R. Biswas, and A. Perdomo-Ortiz, *Physical Review X* **7**, 041052 (2017).
- [33] W. Huggins, P. Patel, K. B. Whaley, and E. M. Stoudenmire, arXiv preprint arXiv:1803.11537 (2018).
- [34] E. Grant, M. Benedetti, S. Cao, A. Hallam, J. Lockhart, V. Stojevic, A. G. Green, and S. Severini, arXiv preprint arXiv:1804.03680 (2018).
- [35] J. R. McClean, J. Romero, R. Babbush, and A. Aspuru-Guzik, *New Journal of Physics* **18**, 023023 (2016).
- [36] A. Berlinet and C. Thomas-Agnan, *Reproducing kernel Hilbert spaces in probability and statistics* (Springer Science & Business Media, 2011).
- [37] K. Mitarai, M. Negoro, M. Kitagawa, and K. Fujii, arXiv preprint arXiv:1803.00745 (2018).
- [38] M. A. Nielsen and I. L. Chuang, *Quantum computation and quantum information* (Cambridge University Press, 2010).

SUPPLEMENTARY MATERIALS

SM (A): VQP FOR GENERAL TRAINING DATA

In the main text, an assumption of the training data $\mathcal{D} = \{(\mathbf{x}_i, y_i)\}_{i=0}^{N-1} \in (\mathbb{R}^{N \times M}, \{-1, 1\}^N)$ is that each example satisfies $\sum_{j=0}^{M-1} |x_{ji}|^2 = 1/N$, with $\forall i \in \{0, 1, \dots, N-1\}$. In this case, the diffusion operator $U_{init} = \mathbb{I} - (H|0\rangle\langle 0|H^\dagger)^{\otimes \lceil \log N \rceil}$ is implemented by applying a Hadamard gate to each index qubit. Such an assumption can be removed by substituting Hadamard gates with $O(\text{poly}(\lceil \log N \rceil))$ blocks of quantum circuits dedicated to learning an amplitude amplification operation.

Amplitude amplification can be viewed as a generalization of Grover search [17]. Specifically, given a dataset $\mathcal{X} = \{\mathbf{x}_1, \mathbf{x}_2, \dots, \mathbf{x}_{2N}\}$, there exists a boolean function f mapping \mathcal{X} into $\{0, 1\}$, with $f(\mathbf{x}_i) \rightarrow \{0, 1\}$, $\forall \mathbf{x}_i \in \mathcal{X}$. The dataset \mathcal{X} can be divided into two subsets, denoted as \mathcal{S}_1 and \mathcal{S}_2 , where $\mathbf{x}_i \in \mathcal{S}_1$ satisfies $f(\mathbf{x}_i) = 1$, and, alternatively, $\mathbf{x}_j \in \mathcal{S}_2$ satisfies that $f(\mathbf{x}_j) = 0$. Suppose that a quantum algorithm \mathcal{A} , that encodes \mathcal{X} into a superposition state $\mathcal{A}|0\rangle^{\otimes N} = \sum_i \alpha_i |\mathbf{x}_i\rangle$ with $\sum_i |\alpha_i|^2 = 1$, exists. Let $P_{\mathcal{S}_1} = \sum_{\mathbf{x}_i \in \mathcal{S}_1} |\alpha_i|^2$. Analogous to the Grover search algorithm, applying two oracles $U_f |\mathbf{x}_i\rangle = (-1)^{f(\mathbf{x}_i)} |\mathbf{x}_i\rangle$ and $U_{init} = -\mathcal{A}\mathbb{I}_0\mathcal{A}^{-1}$ with $\mathbb{I}_0 = (\mathbb{I} - |0\rangle^{\lceil \log N \rceil}\langle 0|^{\lceil \log N \rceil})$, $\Theta(1/\sqrt{P_{\mathcal{S}_1}})$ times, an element in \mathcal{S}_1 will be found with a probability close to 1.

Given a general training data $\mathcal{D} = \{(\mathbf{x}_i, y_i)\}_{i=0}^{N-1}$, a normalized dataset $\mathcal{D}_G = \{(\mathbf{x}_i/\mathcal{N}, y_i)\}_{i=0}^{N-1} \in (\mathbb{R}^{N \times M}, \{-1, 1\}^N)$, with $\mathcal{N} = \sum_{j=0}^{M-1} \sum_{i=0}^{N-1} |x_{ji}|^2$, is constructed before encoding it to a quantum state. We then use amplitude amplification operation \mathcal{A} to construct the diffusion operator $U_{init} = -\mathcal{A}\mathbb{I}_0\mathcal{A}^{-1}$, where \mathcal{A} can be effectively implemented by a parameterized quantum circuit.

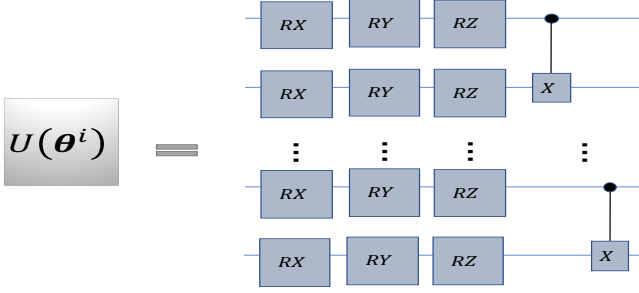


FIG. 5: Suppose that i -th block $U(\theta^i)$ interacts with $\lceil \log M \rceil$ qubits. Three trainable parameterized gates, RX, RY and RZ, are firstly applied to each qubit, followed by $\lceil \log M \rceil - 1$ CNOT gates.

SM (B): PARAMETERIZED QUANTUM CIRCUITS AND OPTIMIZING METHOD

The parameterized quantum circuit (PQC), which is composed of trainable single qubit gates (e.g., the rotation gates along three axis) and CNOT gates, is employed to construct U_f and U_{dis} . As a promising scheme for NISQ devices, PQC has been extensively investigated for accomplishing the generative [30–32] and discriminative [22, 23, 33, 34] tasks via variational hybrid quantum/classical algorithms [35]. One typical PQC is called the multiple-layer PQC (MPQC), where the arrangement of quantum gates in each block is identical [30, 31]. Denote the operation generated by the i -th block as $U(\theta^i)$, and let the number of trainable parameters be proportional to the number of qubits $|\theta^i| \sim O(\text{poly}(\log M))$. Denote the generated quantum state from MPQC as $|\Psi\rangle = \prod_{i=1}^L U(\theta^i) |0\rangle^{\otimes \lceil \log M \rceil}$, where the L is the total number of blocks. In this Letter, MPQC that is employed to construct U_f and U_{dis} has the circuit arrangement as shown in Figure 5. Consequently, the total number of trainable parameters in our VQP is $3\lceil \log M \rceil(L_1 + L_2)$.

The training method used in VQP is a hybrid quantum-classical algorithm. Specifically, a classical optimizer iteratively updates the parameters $\{\theta^i\}$ of all blocks, which enforce U_f and U_{dis} to learn their target forms. Mathematically, suppose the entangled quantum state of the index and feature qubits is $|\Psi\rangle_{F,I} = \sum_{i=1}^N \sum_{j=1}^M \alpha'_{ji} |j\rangle |i\rangle$, where α'_{ji} represents the probability amplitude of the state $|j\rangle |i\rangle$ with $\sum_{j,i} |\alpha'_{ji}|^2 = 1$. The probability for the index $i \in \{1, 2, \dots, N\}$ is

$$q(x = i) = \sum_{j=1}^M |\langle i, j | \Psi \rangle_{F,I}|^2. \quad (8)$$

For the purpose of sampling the mislabeled index k with the highest probability, the targeted probability distribution is set to be $p(x = k) = 1$ and zero otherwise. In VQP, the maximum mean discrepancy (MMD) loss is employed as the classical optimizer, which measures the distance

between $q(x)$ and $p(x)$ by updating θ . The MMD loss is defined as

$$\begin{aligned} \mathcal{L} &= \left\| \sum_x q(x) \phi(x) - \sum_x p(x) \phi(x) \right\|^2 \\ &= \mathbb{E}_{x \sim q(x), y \sim q(x)} [K(x, y)] - 2 \mathbb{E}_{x \sim q(x), y \sim p(x)} [K(x, y)] + \mathbb{E}_{x \sim p(x), y \sim p(x)} [K(x, y)], \quad (9) \end{aligned}$$

where $\phi(x)$ maps the data x to a high-dimensional reproducing kernel Hilbert space and $K(x, y) = \phi(x)\phi(y)^\top$ is a Gaussian kernel [36], and the mixture Gaussian kernel is $K(x, y) = \exp(-|x - y|^2/2\sigma_i)$ with the bandwidth σ_i . In the training process, a gradient and unbiased estimation method, proposed by [37], is employed to minimize the MMD loss. The learning rate r used in gradient method is a hyper-parameter that controls how quick the parameters are updated, i.e., $\theta = \theta - r * \partial \mathcal{L} / \partial \theta$.

SM (C): PROOF OF THEOREM 1

Proof. Since U_{dis} only locally interacts with the feature register and the number of blocks is limited, the fully disentangled state in Eqn. (3) cannot be generated. Instead, w.l.o.g., the generated state has the following form

$$\begin{aligned} &(U_{dis} \otimes \mathbb{I}) U_f |\Phi^k\rangle_{F,I} \quad (10) \\ &= (\sqrt{1-\epsilon} |\Phi^k\rangle_F - \sqrt{\epsilon} |\Phi^{k\perp}\rangle_F) \otimes \sqrt{\frac{b}{N}} |B\rangle \\ &\quad + (\sqrt{1-\epsilon} |\Phi^k\rangle_F - \sqrt{\epsilon} |\Phi^{k\perp}\rangle_F) \otimes (-\sqrt{\frac{a}{N}} |A\rangle), \end{aligned}$$

where $b = |B|$, $a = |A|$, and $|\Phi^{k\perp}\rangle$ represents the orthogonal complement to $|\Phi^k\rangle$.

Applying U_{init} to Eqn. (10) yields

$$U_{init}(U_{dis} \otimes \mathbb{I}) U_f |\Phi^k\rangle_{F,I} = M_\epsilon \begin{bmatrix} |\Phi^k\rangle_F \\ |\Phi^{k\perp}\rangle_F \end{bmatrix} \otimes M \begin{bmatrix} |B\rangle \\ |A\rangle \end{bmatrix}, \quad (11)$$

where $M_\epsilon = [-\sqrt{1-\epsilon} \ \sqrt{\epsilon}]$. Let $\sqrt{\epsilon} = \sin \gamma$. After S iterations, the generated state of $\prod_{i=1}^S U_{init}^i U_{dis}^i U_f^i |\Phi^k\rangle_{F,I}$ can be expressed as

$$\begin{aligned} &\prod_{i=1}^S (\mathbb{I} \otimes U_{init}^i) (U_{dis}^i \otimes \mathbb{I}) U_f^i |\Phi^k\rangle_{F,I} \\ &= ((-1)^S \cos^S \gamma |\Phi^k\rangle_F + \sin^S \gamma |\Phi^{k\perp}\rangle_F) \otimes \\ &\quad (\cos(2S+1)\theta |B\rangle + \sin(2S+1)\theta |A\rangle). \quad (12) \end{aligned}$$

Therefore, the sampling probability of the targeted state $|\Phi^k\rangle_F |A\rangle$ is $|(-1)^S \cos^S \gamma \sin(2S+1)\theta|^2 = |1 - \epsilon|^S |\sin(2S+1)\theta|$. \square

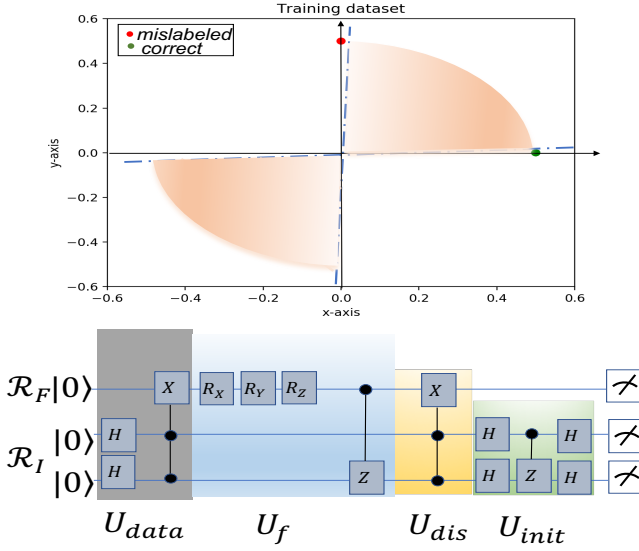


FIG. 6: (a) The dataset \mathcal{D} . (b) The quantum circuit implementation of VQP.

SM (D): A TOY EXAMPLE

Now we devise a toy model of VQP, where the analytic result can be calculated and compared with the simulation results. Specifically, the dataset \mathcal{D} contains four training examples with the number of features $|\mathbf{x}_i| = 2$, defined as $\mathcal{D} = \{(\mathbf{x}_i, y_i)\}_{i=1}^4$ with $(\mathbf{x}_1, y_1) = (1, 0, 1)$, $(\mathbf{x}_2, y_2) = (1, 0, 1)$, $(\mathbf{x}_3, y_3) = (1, 0, 1)$, and $(\mathbf{x}_4, y_4) = (0, 1, -1)$, respectively. The fourth example is selected as the mislabeled example, where the training data \mathcal{D}_4 is illustrated in Figure 6 (a). Notably, any hyperplane that locates at the orange region can accurately classify the training data.

In the training process, the L_1 is setting to be 1. Since the number of feature is 2, where one feature qubit is sufficient, the block of U_{L_1} does not contain CNOT gate and only contains three rotational single qubit gates R_X , R_Y , and R_Z . For accessing U_{L_1} to see what decision rule has been learned after optimizing, the disentangled operator U_{dis} is explicitly predefined by a Toffoli gate to disentangle the entanglement between the feature register and the index register. The implementation quantum circuits is illustrated in Figure 6 (b).

Analytically, as proved in [38], with total 4 examples and 1 mislabeled data, the objection is expected to be sampled after one iteration using Grover search. Mathematically, the quantum state of the training data \mathcal{D}_4 is

$$|\Phi^4\rangle_{F,I} = \frac{1}{2} (|0\rangle_F |00\rangle_I + |0\rangle_F |01\rangle_I + |0\rangle_F |10\rangle_I + |1\rangle_F |11\rangle_I) .$$

For the purpose of activating the feature qubit. i.e.,

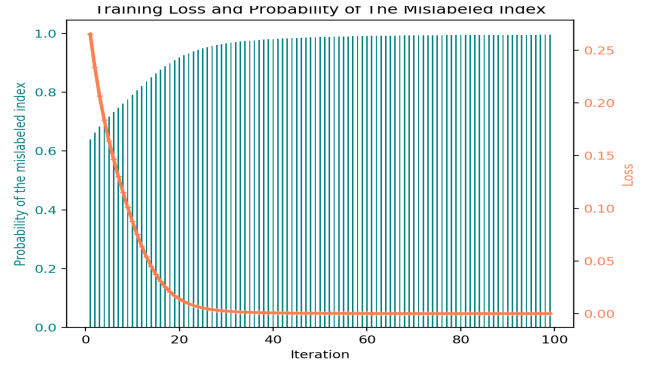


FIG. 7: The training loss and probability of the mislabeled index.

$|1\rangle_F$ only for the mislabeled index state $|11\rangle_I$, all trainable parameters of U_{L_1} is expected to be zero, acting as Identity gate. Then, the generated state after interacting with U_f is denoted as $U_f |\Phi^k\rangle = |0\rangle_F |00\rangle_I + |0\rangle_F |01\rangle_I + |0\rangle_F |10\rangle_I - |1\rangle_F |11\rangle_I$. Then after applying U_{dis} and U_{init} , the quantum state can be expressed as $U_{init} U_{dis} U_f |\Phi^k\rangle = |0\rangle_F |11\rangle_I$, where the sampling probability of $|11\rangle_I$ is expected to be 1.

The training loss function is illustrated in the Figure 7, where the probability of sampling the mislabeled data reaches 99.5% after 100 iterations. The three trainable parameters are 0.02, 0.01, and 0.16, which approximate the identity gates as we expected.

The test dataset \mathcal{D}_{test} contains 200 examples, where each example (\mathbf{x}_i, y_i) satisfies $\mathbf{x}_i = \{\cos(\theta_i), \sin(\theta_i)\}$, with $\theta_i \in [0, 2\pi)$, and $y_i = -1$ if $\theta_i \in [0, \pi)$ while $y_i = 1$ if $\theta_i \in [\pi, 2\pi)$. With setting the threshold C_T as 0.55, 0.6, and 0.65, respectively, the classification accuracy are 96.00%, 98.50%, and 99.50%, as shown in Figure 8 (a) (b) and (c).

The decision rule learned by VQP, as highlighted by blue lines, can be treated as a distance classifier. If the input is close to the decision boundary, the prediction is more sensitive to the threshold and the confidence is low. In contrast, the input that is close to the mislabeled data can be accurately predicted with a high confidence.

Since the learned U_{L_1} can be treated as an Identity gate, it cannot distinguish $-\mathbf{x}_i$ and \mathbf{x}_i with directly measuring $U_f |\mathbf{x}_i\rangle$ and $-U_f |\mathbf{x}_i\rangle$. As shown in Figure 8 (d), the probability of conditionally seeing $F_1 = 1$ is symmetric, where the phase difference is vanished. (That is why we employ a SWAP test in prediction method.)

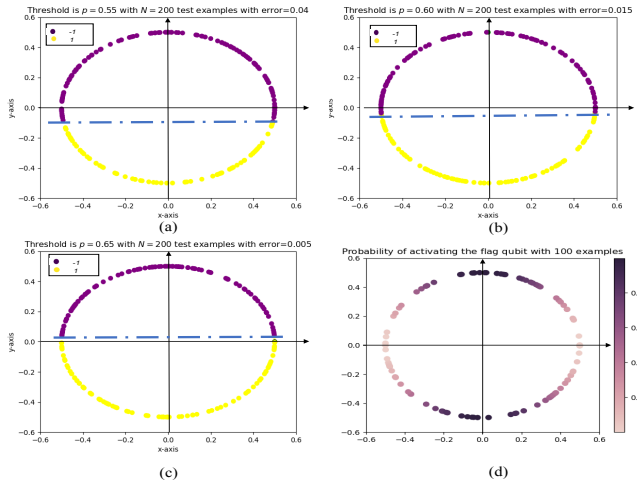


FIG. 8: Figure (a) (b) (c) show training loss and probability of the mislabeled index with different thresholds. Figure (d) illustrates the probability to activate the first qubit of the feature register for different inputs.